Design and Manipulation of a Minimalistic Hydrocarbon Nanocar on Au(111)

Ana Barragán, Tomás Nicolás-García, Koen Lauwaet, Ana Sánchez-Grande, José I. Urgel, Jonas Björk, Emilio M. Pérez, David Écija

RESEARCH ARTICLE

Design and Manipulation of a Minimalistic Hydrocarbon Nanocar on Au(111)

Ana Barragán,[a] Tomás Nicolás-García,[a] Koen Lauwaet,[a] Ana Sánchez-Grande,[a,b] José I. Urgel,[a] Jonas Björk,*[c] Emilio M. Pérez*[a] and David Écija*[a]

[a] Dr. A. Barragán, T. Nicolás-García, Dr. K. Lauwaet, Dr. A. Sánchez-Grande, Dr. J. I. Urgel, Dr. E. M. Pérez, Dr. D. Écija
IMDEA Nanoscience Institute
C/ Faraday 9, Campus de Cantoblanco, 28049 Madrid (Spain)
E-mail: emilio.perez@imdea.org, david.ecija@imdea.org
[b] Dr. A. Sánchez-Grande
Institute of Physics of the Czech Academy of Science
CZ-16200 Praha (Czech Republic)
[c] Dr. J. Björk
Department of Physics, Chemistry and Biology
IFM, Linköping University, 581 83, Linköping (Sweden)
Email: jonas.bjork@liu.se

Supporting information for this article is given via a link at the end of the document.

Abstract: *Nanocars are carbon-based single-molecules with a precise design that facilitates their atomic-scale control on a surface. The rational design of these molecules is important in atomic and molecular-scale manipulation to advance the development of molecular machines, as well as for a better understanding of self-assembly, diffusion and desorption processes. Here, we introduce the molecular design and construction of minimalistic nanocar. They feature an anthracene chassis and four benzene derivatives as wheels. After sublimation and adsorption on an Au(111) surface, we show controlled and fast manipulation of a nanocar along the surface using the tip of a scanning tunneling microscope (STM). The mechanism behind the successful displacement is the induced dipole created over the nanocar by the STM tip. We utilized carbon monoxide functionalized tips both to avoid decomposition and accidentally picking the nanocars up during the manipulation. This strategy allowed thousands of maneuvers to successfully win the Nanocar Race II championship.*

Introduction

The first examples of synthetic molecular machines were often directly inspired by macroscopic machines with examples such as molecular pistons, [1] clutches, [2] wheelbarrows, [3] and elevators. [4] Later, the field turned to Nature for inspiration, both in terms of structure and function, and produced some of the most advanced machines, including molecular motors, [5,6] pumps, [7,8] and molecular synthesizers. [9,10] Nanocars [11–13] fall within the family of molecular machines that mirror macroscopic counterparts, with the focus on understanding and controlling the manipulation of matter at the molecular scale. So far, the mechanisms behind the controlled translation or rotation of nanocars on surfaces have been mainly explained in terms of the inelastic tunneling electrons, [14–16] or the generated electric field between the STM tip and the molecule. [17–19]

In order to highlight and drive the advances in the control of individual molecules on surfaces at the nanoscale, the first International Nanocar Race (INR) took place in 2017. [20] For the second edition of the INR, the winner would be the team covering the longest distance possible on an Au(111) surface in a 24 hours single drive. The vehicles are nanocars, molecules adsorbed on an Au(111) surface under ultra-high vacuum (UHV) conditions and driven by their interaction with the STM tip. Several synthetic strategies to obtain molecular-scaled-controlled nanocars have been reported during the last years, [12,21–30] with some of them showcased in the first INR. [20] In this work, we show our approach to design and control a nanocar that went on to win the second edition of the INR.

The starting point of our design process was to follow the recommendations reported by the winners of the first edition of the INR. [31,32]. Among these advices, we paid special attention to maintain a reduced overall weight of our nanocar, minimize nanocar-surface interactions, and enhance structural stability after sublimation. With these ideas in mind, we proposed a new family of minimalistic nanocars, with distinguishable front and rear. We opted for an anthracene unit as chassis equipped with four aromatic rings as wheels (see Figure 1 for a schematic representation of the nanocars). These nanocars are composed of around 70 atoms with molecular weights ~500 g/mol. Due to steric intramolecular hindrance, the four peripheral wheels are expected to be tilted with respect to the plane of the anthracene moiety, thus limiting the interactions between the nanocar and the gold circuit to just van der Waals interactions. Before settling on our final design, the rear wheels were synthesized with three different substituents, as shown in Figure 1 and Scheme 1, to fine-tune their properties, as well as the response to the STM tip at the tunneling junction. **Nanocar-Me**, which was finally selected for the race, shows outstanding stability during thermal sublimation and STM manipulation, taking advance of its molecular structure that comprises only relatively strong carbon-carbon (C–C) and carbon-hydrogen (C–H) bonds.

Some nanocar molecules have been designed with a high permanent dipole moment to ensure the lateral movement on the surface. [33–35] **Nanocar-Me** only exhibits a small built-in dipole moment, even though there is an asymmetry between rear and

front wheels. As explained below, the main responsible for the manipulation mechanism is, instead, the induced dipole moment of the molecule created with the electric field of the STM tip when the tip is brought into close proximity to the nanocar, and a high bias is applied. Using a low bias, the induced dipole moment is lower and the nanocar can be stably imaged.

As mechanical pushing is not allowed in the INR, we had to minimize mechanical interactions between the tip and the nanocar while still allowing for the creation of a sufficiently large electric field between the STM tip and the sample to induce the needed dipole. Unfortunately, these two features are mutually exclusive when using metallic tips. Therefore, to avoid "picking-up" events, we have employed CO-functionalized STM tips. Coating the tip with a CO molecule makes the tip passivated, flexible and less reactive, being in our case particularly useful because of the low molecule-surface interaction. Following this passivation, the tip apex is less reactive, which allows the tip to be located much closer to the surface without destroying the tip or picking up attracted nanocars. Since the electric field is inversely proportional to the distance between the tip and the sample, by bringing closer the tip to the surface, higher electric fields are generated and, consequently, attracting, but not catching, them.[36] Altogether, these CO functionalized tips, allow to induce higher dipoles at the nanocars and a controlled lateral manipulation mechanism on the Au(111) surface. Consequently, we were able to cover long distances in a controlled manner. Furthermore, the combination of these experiments and theoretical calculations has resulted in a comprehensive study of this new family of molecules on surfaces, which will contribute to the development of future generations of nanocars as well as provide insights into surface science and molecular machinery.

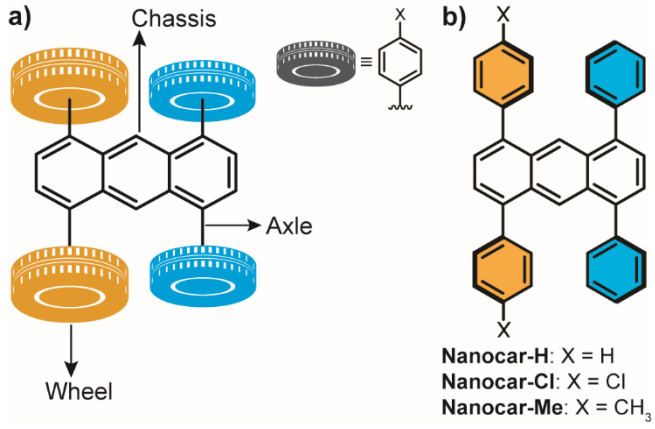

Figure 1. a) Schematic illustration of a minimalistic anthracene-based nanocar. b) Chemical structure of the synthetized nanocars.

Results and Discussion

Three minimalistic anthracene-based nanocars were prepared following the synthetic procedure depicted in Scheme 1, where thanks to a sequence of [4+2] cycloadditions, we were able to desimetrize the front and rear ends of the anthracene chassis. The procedure started with the preparation of bisaryne precursor **1**, [37] which is the core of the anthracene backbone. On the other hand, the wheels were inserted through diphenylfuran derivatives (**4a-c**) that can be readilly synthetized by Suzuki cross-coupling reaction between dibromofuran (**2**) and the corresponding boric acid (**3a-c**). The key point of the synthetic procedure was the controlled generation of the triple bond in **1**, based on the fact that CsF is only slightly soluble in acetonitrile. [38] This allowed us to control the generation of the aryne to avoid bisaddition of the first set of wheels and favor formation of the common intermediate **5**. Thereby, we were able to tune the built-in dipole moment of our anthracene-based nanocars as result of the different relative inductive effect of the substituents strategically placed at other side of the chassis with another pair of wheels by a subsequent [4+2] cycloaddition, to give the precursors **6a-c**. Finally, the oxygen atoms were removed to yield the aromatic nanocars.

In Table 1 are estimated by density functional theory (DFT) the built-in dipole moments of both asymmetric **nanocar-Cl** and **nanocar-Me** (0.51 and 0.13 Debye, respectively), which are smaller than previously reported nanocars. [33–35] To discern between polarity and polarizability, the symmetric **nanocar-H** with a negligible dipole moment (0.006 Debye) was employed as a reference.

Table 1. Theoretical dipole moments of the nanocars estimated by DFT calculations.

Nanocar	Substituent	μ (Debye)
Nanocar-H	-H	0.01
Nanocar-Me	-CH_3	0.13
Nanocar-Cl	-Cl	0.51

First, we decided to test the most polarized **nanocar-Cl**, equipped with chlorine atoms as electron-withdrawing substituents, to generate a permanent dipole moment on the molecule. Figure 2a shows the adsorption of a submonolayer coverage, where the nanocars self-assemble into islands stabilized through supramolecular interactions. However, as observed in Figure 2b, some of the molecules have been decomposed after sublimation on the Au(111) surface, kept at room temperature, by losing one or two wheels, probably due to the interaction between the chlorine atoms and the gold surface. Furthermore, the controlled manipulation of the few intact molecules was not possible.

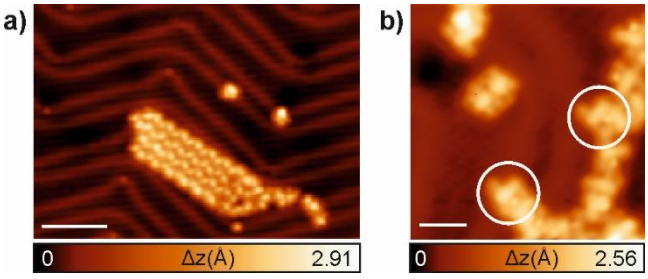

Figure 2. Adsorption of **nanocar-Cl** on Au(111). a) STM image showing a self-assembled nanocar island. V_b = -3.0 V, I_t = 150 pA, scale bar = 8 nm. b) High-resolution STM image showing some nanocars with missing wheels (see white circles). V_b = 0.5 V, I_t = 5 pA, scale bar = 2.1 nm.

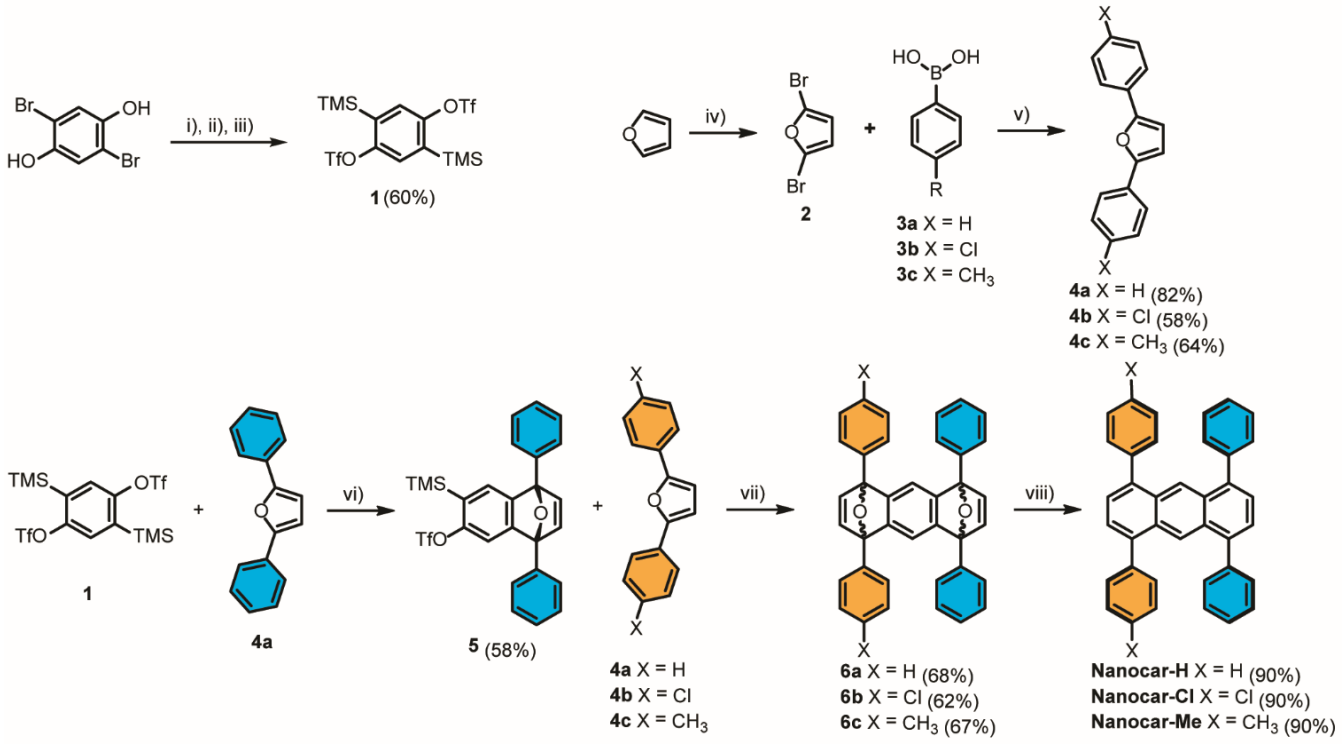

Scheme 1. Synthesis of nanocars. Reagents and conditions: i) TMSCl, Et_3N, THF, r.t. 1 h; ii) TMSCl, *n*-BuLi, THF, -78 ºC to r.t. 2 h; iii) Tf_2O, *n*-BuLi, Et_2O, -78 ºC to 0 ºC to r.t. 3 h; iv) Br_2, DMF, 20 ºC, 12 h; v) Na_2CO_3, toluene, H_2O, $Pd(PPh_3)_4$, 120 ºC, 24 h; vi) CsF, MeCN, r.t. 4 h; vii) CsF, MeCN, r.t. 3 h; viii) TMSCl, NaI, MeCN, DCM, 12 h. The permanent dipole moment of the nanocars can be tuned by properly combining functional groups with different relative inductive effects on the external side of the molecule.

Therefore, we went back to the pit stop and decided to try with a nanocar equipped with a more robust functional group, i.e. $–CH_3$, namely **nanocar-Me**, thus reducing the possible reactivity of the molecule at the expense of a lower built-in dipolar moment generated by the slightly inductive effect of the methyl group.

In the remainder of this paper, we show that **nanocar-Me** was sublimed successfully onto the Au(111) surface, and that it could be driven in a highly controlled manner on this surface.

Figure 3a illustrates an overview STM image obtained using a CO-functionalized tip of the sample after the deposition of a low submonolayer coverage of **nanocar-Me** on the Au(111) surface. As the nanocars have been designed for low molecule-surface interaction, and the deposition is performed with the Au(111) at room temperature, we expect the nanocars to be highly mobile. This is reflected in the finding that the nanocars are located at two stable sites. Either they are located on the highly reactive elbows of the Au(111) herringbone surface reconstruction, or they diffuse until they are incorporated into self-assembled island consisting of nanocars parked together along the face centered cubic (FCC) region of the herringbone reconstruction. Individual molecules for racing are obtained from the self-assembled islands by tip-induced lateral manipulation, as it is explained in Figure S3. Even at low temperatures (4 K), the molecules remain quite mobile under STM inspection and have to be measured using a CO-functionalized tip to avoid any undesired movement (Figure S4).

Figure 3b shows a zoomed-in STM image of an isolated nanocar, where it is possible to discern an elongated central part, attributed to the anthracene chassis, and the four peripheral wheels. We are also able to differentiate between benzene (thin) and toluene (bulky) moieties, by a comparison with DFT calculated images (Figure 3d).

Theoretical calculations were performed for several adsorption configurations of **nanocar-Me** considering the anthracene chassis direction with respect to: i) the high-symmetry directions of the surface, ii) the adsorption site, and iii) the orientation of the benzene rings. The two most stable configurations are presented and compared in Figure S5. They have been found below the accuracy of the calculations (within 2 meV). Among them, the STM simulated image of the configuration presented in Figure 3c gives a better agreement with the experimental STM images, both resembling a perfect cartoon-like car shape (Figures 3b and d).

DFT calculations confirm that the aromatic wheels are not co-planar with the anthracene chassis, due to steric interactions. The wheels slightly lift the chassis from the Au(111) substrate, thereby minimizing the interaction between the chassis and the substrate (Figure 3c, bottom), which adsorbs almost parallel to the surface, with a slight inclination with respect the Au(111) plane. As previously mentioned, keeping this interaction low was one of the key points of our design, as polyaromatic π-molecules tend to interact with the metallic surface, hampering the mobility of the molecule.

Notably, most of the considered adsorption configurations are found with a difference of only 10 meV, pointing that the molecule can easily be moved along the surface under a weak external

stimulus. It is also expected that the phenyl rings will keep their orientation when displacing on the surface, because switching them is difficult, due to steric hindrance. It is noteworthy that due to the interaction of the **nanocar-Me** with the gold surface, the final configuration of the phenyl rings is slightly different when compared to the gas-phase conformation (see figure S6), though still out of the plane.

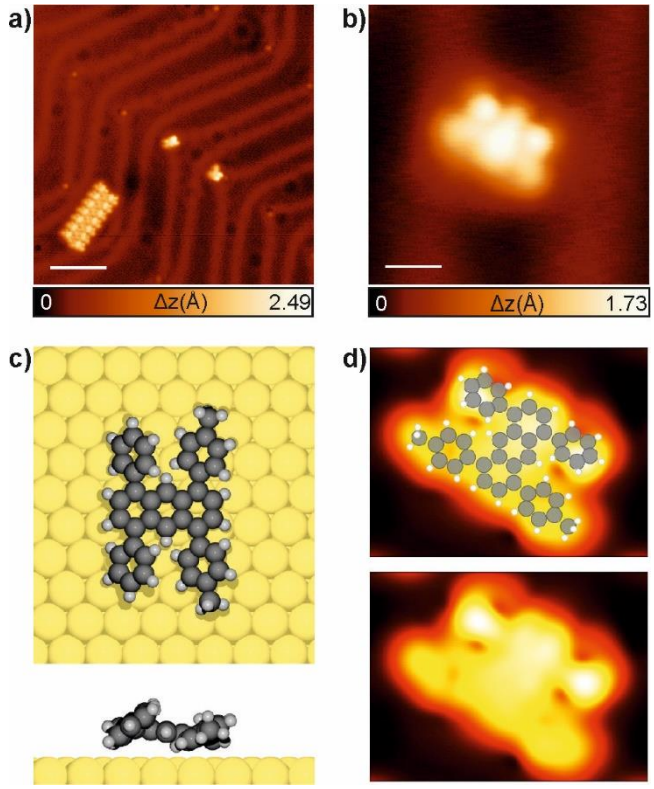

Figure 3. a) STM image of a submonolayer coverage of **nanocar-Me** species on Au(111). V_b = 0.2 V, I_t = 5 pA, scale bar = 6 nm. b) STM image of an isolated nanocar molecule in which intramolecular features are distinguished. V_b = 0.2 V, I_t = 5 pA, scale bar = 0.8 nm. c) DFT calculation of one of the two most stable adsorption configuration of **nanocar-Me** on Au(111), which gives the best fit to the contrast with the experimental STM image. d) Simulated STM image of **nanocar-Me** (local density of states at the Fermi level), which can be compared with an experimental constant current STM at low bias, providing an excellent match.

Once individual molecules are obtained, we have developed a tip-induced electrical field gradient as propulsion mechanism for the controlled surface diffusion along the Au(111) surface. It is important to mention that our driving mechanism works independently of either the molecular adsorption position (except those located at the herringbone elbows, which act as pinning centers), or the moving direction (along and across the herringbone lines).

A translation event step is shown in Figure 4 and proceeds as follows: the CO-functionalized tip is located at the position where we want to displace the molecule, at a lateral tip-molecule distance around 1.5 - 2 nm, as represented by the white spot in Figure 4a. At that local tip position, with standard STM conditions (0.2 V and 5 pA), the feedback loop is opened, and the bias applied to the tip is progressively increased to 2.2 V, in 0.1 V steps, while recording the current as a function of the time. After some instabilities, a sudden jump to a value of at least 2 nA in the tunneling current indicates that a manipulation event has taken place (see Figure 4c). As it will be explained in the next paragraphs, this sudden increase of the tunneling current is attributed to the relocation of the molecule, which is now present in the tunnel junction. Notably, the nanocar is attracted towards the tip due to the electric field between tip and sample that induces a dipole on the molecule.

After the appearance of the translation event, if we want to see the new position of the molecule with respect to the surface, the tunneling parameters are set back to non-perturbative conditions, the feedback loop is closed and a new constant current STM image is acquired. As observed in Figure 4b, after the manipulation event, the molecule is located with one of its two front wheels (benzene moieties) where the tip was positioned during the translation event.

As the current versus time is a good indicator of a successful translation event, the tip-molecule attraction process can be repeated without imaging in between. By performing several consecutive translation steps without closing the feedback loop and scanning the molecular position each time the driving becomes much more time efficient. [25] Due to the new rules introduced in the second edition of the INC, there was an upper limit to how many translations could be performed between consecutive images.

In order for a translation event to be successful, the tip should not be placed too far from the molecule in the lateral plane. A good indication to check if this distance is correct is again the current versus time trace. When the tip is placed too far, the current will remain low (< 0.1 nA), and stable. However, bringing the tip in the optimal range for the displacement of the nanocar, the current will be higher and fluctuating (Figure 4d). Therefore, if the current signal is high and fluctuating, or reflects the sudden jump to around 2 nA, we know that the molecule is below the tip and the next driving steps can be done along the desired moving direction.

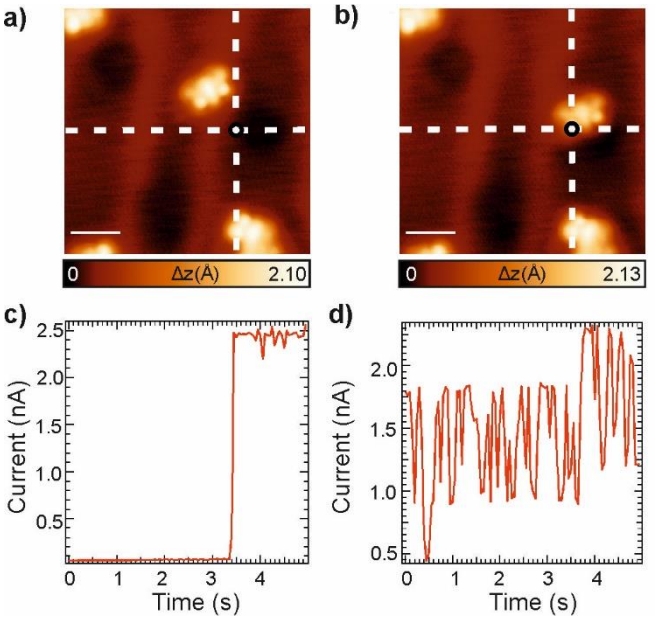

Figure 4. Driving mechanism of **nanocar-Me**. a,b) High-resolution STM images before and after a manipulation event, respectively (V_b = 0.2 V, I_t = 5 pA, scale bars = 1.7 nm). The position of the STM tip is indicated by the white dot. c) Current versus time trace while increasing the bias voltage with the feedback loop open. The jump indicates the translation event from a) to b). d) Current instabilities typically observed when the molecule is close to the tip, in the optimal range for translation.

A complete manipulation sequence overcoming an obstacle absorbed on a herringbone elbow is presented in Figure 5. The nanocar is able to overcome the obstacle by following the trajectory indicated by the yellow arrow, showing that we can drive it in a controllable fashion following any desired track (see also movie of GIFs in the Supporting Information).

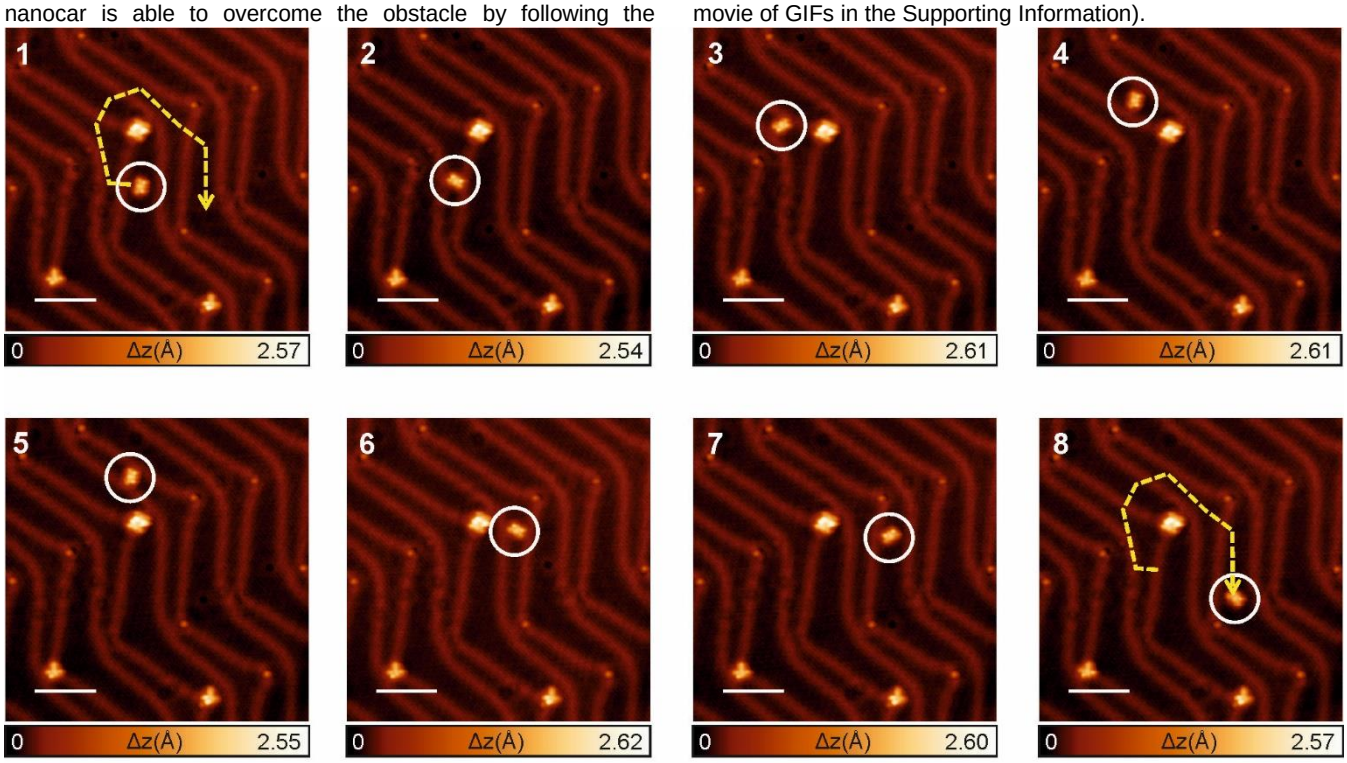

Figure 5. Series of STM images showing the driving of a **nanocar-Me** around an elbow of the herringbone reconstruction of Au(111). The positions of the driven nanocar are marked with a white circle in each panel, while the final molecular path is shown by the yellow arrow. V_b =0.2V, I_t = 5pA, scale bars = 6 nm.

So far, we have demonstrated how we can maneuver a relatively chemically inert molecule with negligible internal dipole moment over Au(111) by creating an electrostatic field between the STM tip and surface. The successful response of the **nanocar-Me** to an external electrostatic field, despite of having very small static dipole moment, becomes clear when considering its *electronic polarizability* – how the dipole moment is affected by an electric field. DFT calculations of the polarizability are summarized in Figure 6, showing significant electronic polarizabilities along all three molecular axes, which could be compared to the mean electronic polarizability of benzene (9.96 Å^3). [39] The relatively large values for our nanocar are expected as the polarizability generally scales linearly with the number of electrons.[39] Importantly, the quite significant values of polarizability means that a dipole moment will be induced in the molecule as a response to the electrostatic field between STM tip and surface, making the molecule attracted towards such field, thus resulting in a net movement under appropriate tunneling parameters.

STM experiments and DFT calculations of a control **nanocar-H** are included in the Supporting info (see section S11). Such nanocar is symmetric and displays a negligible static dipole moment, while featuring polarizability values of the same order than **nanocar-Me**. Importantly, **nanocar-H** can be manipulated along the Au(111) surface in a similar way than reported above, thus reinforcing the suggested dominant mechanism for manipulation based on induced polarizability, without the need of a static dipole moment.

In addition, negative biases for both nanocars, typically lower than -1 eV (to avoid influence of frontier orbitals), also generate attractive manipulation events (though with less average success than positive biases), which would be expected for a dominant mechanism of attraction based on induced polarizability.

Finally, it is worth to highlight that we cannot rule out that inelastic tunneling phenomena arising from hot electrons could play a minor role in the overall mechanism of attraction (see Supporting Information for an electronic description of nanocars **-H** and **-Me**).

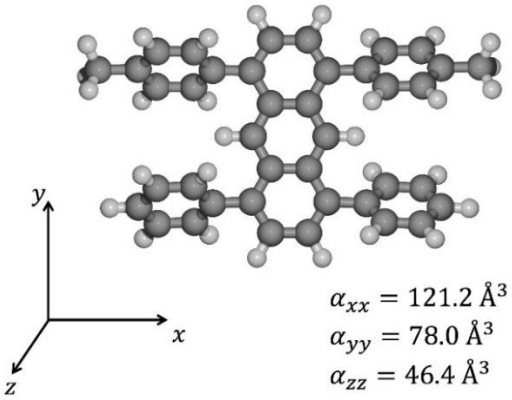

Figure 6. Calculated polarizabilities along the three molecular axes of **nanocar-Me**.

Conclusion

In this work, we have presented the design, synthesis, sublimation and tip-induced manipulation of a minimalistic anthracene-based nanocar operated through STM on Au(111). Apart from the anthracene central chassis, the nanocar features benzene and toluene wheels at the front and rear, respectively. By a combination of DFT theoretical simulations and STM inspection, the mechanism of its movement has been unveiled. The manipulation and translation control of **nanocar-Me** on the Au(111) surface at the single-molecule scale is possible by taking advantage of the attraction between the CO-functionalized STM tip and the induced electrical dipole at the nanocar. The reliable nature of this control thanks to CO-functionalized tips made our nanocar a winning participant in the second edition of the INR.
We envision that our study will provide insights for the future design and manipulation of nanocars on surfaces, thus opening avenues in molecular machinery.

Experimental Section

Synthetic procedure in SI. Racing experiments were performed with a custom-designed low-temperature microscope, under UHV conditions, with a base pressure below 4×10^{-10} mbar. The system is equipped with STM/AFM capabilities from Scienta Omicron, and it is operated with Matrix control electronics. The Au(111) surface was prepared by cycles of 10 minutes Ar^+ ion sputtering (E = 1.5 keV, I = 10 μA) and subsequent annealing (740 K) under UHV conditions. **Nanocar-Cl** was sublimed at 177 ºC, **nanocar-Me** at 165 ºC and **nanocar-H** at 180 ºC, while the surface was held at room temperature. For the thermal deposition, we use a Kentax TCE-BSC evaporator. A quartz micro-balance (LewVac) was used to check the deposition rates of the molecules. Once prepared, the sample was transferred within the UHV system to the microscope where it was cooled down to 4.3 K for measurements. Before starting the STM experiments, to obtain CO-functionalized tips, CO molecules were dosed for few seconds at a pressure of $1 \cdot 10^{-8}$ mbar. For molecular manipulation see Supplementary Info for details. The STM images were analysed using WSxM.[40]

Acknowledgements

The authors acknowledge the European Research Council (ERC CoG ELEC-NANO nº766555), the Comunidad de Madrid (project QUIMTRONIC-CM (Y2018/NMT-4783 and P2018/NMT-4367), and the Ministerio de Ciencia e Innovación (PID2019-108532GB-I00, CTQ2017-86060-P and PID2020-11666RB-I00). IMDEA Nanociencia thanks support from the "Severo Ochoa" Programme for Centers of Excellence in R&D (MINECO, GrantSEV-2016-0686). J.I.U. thanks the funding from the European Union'sHorizon 2020 research and innovation programme under the MarieSkolodowska-Curie grant agreement No. [886314]. J.B. acknowledges funding from the Swedish Research Council and the Swedish Government Strategic Research Area in Materials Science on Functional Materials at Linköping University (Faculty Grant SFO-Mat-LiU no. 2009 00971). Computational resources were allocated by the Swedish National Infrastructure for Computing and carried out at the National SupercomputerCentre, Sweden.

Keywords: Nanocars • Molecular machinery • Scanning tunneling microscopy • [4+2] cycloaddition

References

[1] P. R. Ashton, V. Balzani, O. Kocian, L. Prodi, N. Spencer, J. F. Stoddart, *J. Am. Chem. Soc.* **1998**, *120*, 11190–11191.
[2] W. Setaka, T. Nirengi, C. Kabuto, M. Kira, *J. Am. Chem. Soc.* **2008**, *130*, 15762–15763.
[3] L. Grill, K.-H. Rieder, F. Moresco, G. Jimenez-Bueno, C. Wang, G. Rapenne, C. Joachim, *Surface Science* **2005**, *584*, L153–L158.
[4] J. D. Badjic, V. Balzani, A. Credi, S. Silvi, J. F. Stoddart, *Science* **2004**, *303*, 1845–1849.
[5] S. P. Fletcher, F. Dumur, M. M. Pollard, B. L. Feringa, *Science* **2005**, *310*, 80–82.
[6] K. Mo, Y. Zhang, Z. Dong, Y. Yang, X. Ma, B. L. Feringa, D. Zhao, *Nature* **2022**, *609*, 293–298.
[7] C. Cheng, P. R. McGonigal, S. T. Schneebeli, H. Li, N. A. Vermeulen, C. Ke, J. F. Stoddart, *Nature Nanotech* **2015**, *10*, 547–553.
[8] D. Thomas, D. J. Tetlow, Y. Ren, S. Kassem, U. Karaca, D. A. Leigh, *Nat Nanotechnol* **2022**, *17*, 701–707.
[9] B. Lewandowski, G. De Bo, J. W. Ward, M. Papmeyer, S. Kuschel, M. J. Aldegunde, P. M. E. Gramlich, D. Heckmann, S. M. Goldup, D. M. D'Souza, A. E. Fernandes, D. A. Leigh, *Science* **2013**, *339*, 189–193.
[10] Y. Qiu, B. Song, C. Pezzato, D. Shen, W. Liu, L. Zhang, Y. Feng, Q.-H. Guo, K. Cai, W. Li, H. Chen, M. T. Nguyen, Y. Shi, C. Cheng, R. D. Astumian, X. Li, J. F. Stoddart, *Science* **2020**, *368*, 1247–1253.
[11] Y. Shirai, A. J. Osgood, Y. Zhao, K. F. Kelly, J. M. Tour, *Nano Lett.* **2005**, *5*, 2330–2334.
[12] C. Joachim, G. Rappene, *ACS Nano* **2013**, *7*, 11–14.
[13] K. Ariga, T. Mori, W. Nakanishi, *Chemistry – An Asian Journal* **2018**, *13*, 1266–1278.
[14] B. C. Stipe, M. A. Rezaei, W. Ho, *Phys. Rev. Lett.* **1998**, *81*, 1263–1266.
[15] T. Komeda, Y. Kim, M. Kawai, B. N. J. Persson, H. Ueba, *Science* **2002**, *295*, 2055–2058.
[16] J. I. Pascual, N. Lorente, Z. Song, H. Conrad, H.-P. Rust, *Nature* **2003**, *423*, 525–528.
[17] S.-W. Hla, *Journal of Vacuum Science & Technology B: Microelectronics and Nanometer Structures Processing, Measurement, and Phenomena* **2005**, *23*, 1351–1360.
[18] L. J. Whitman, J. A. Stroscio, R. A. Dragoset, R. J. Celotta, *Science* **1991**, *251*, 1206–1210.
[19] F. Massee, Y. K. Huang, M. Aprili, *Science* **2020**, *367*, 68–71.
[20] G. Rapenne, C. Joachim, *Nat Rev Mater* **2017**, *2*, 1–3.
[21] G. Vives, J. M. Tour, *Acc. Chem. Res.* **2009**, *42*, 473–487.
[22] R. Pawlak, T. Meier, N. Renaud, M. Kisiel, A. Hinaut, T. Glatzel, D. Sordes, C. Durand, W.-H. Soe, Baratoff, C. Joachim, C. E. Housecroft, E. C. Constable, E. Meyer, *ACS Nano* **2017**, *11*, 9930–9940.
[23] M. Li, S. Li, K. Zhang, X. Chi, H. Zhou, H.-B. Xu, Y. Zhang, Q. Li, D. Wang, M.-H. Zeng, *Nanoscale* **2021**, *13*, 16748–16754.
[24] G. J. Simpson, V. García-López, A. Daniel Boese, J. M. Tour, L. Grill, *Nat Commun* **2019**, *10*, 4631.
[25] R. Ohmann, J. Meyer, A. Nickel, J. Echeverria, M. Grisolia, C. Joachim, F. Moresco, G. Cuniberti, *ACS Nano* **2015**, *9*, 8394–8400.
[26] W.-H. Soe, Y. Shirai, C. Durand, Y. Yonamine, K. Minami, X. Bouju, M. Kolmer, K. Ariga, C. Joachim, W. Nakanishi, *ACS Nano* **2017**, *11*, 10357–10365.
[27] P.-L. E. Chu, L.-Y. Wang, S. Khatua, A. B. Kolomeisky, S. Link, J. M. Tour, *ACS Nano* **2013**, *7*, 35–41.
[28] J. Godoy, G. Vives, J. M. Tour, *Org. Lett.* **2010**, *12*, 1464–1467.
[29] P.-T. Chiang, J. Mielke, J. Godoy, J. M. Guerrero, L. B. Alemany, C. J. Villagómez, A. Saywell, L. Grill, J. M. Tour, *ACS Nano* **2012**, *6*, 592–597.
[30] T. Kudernac, N. Ruangsupapichat, M. Parschau, B. Maciá, N. Katsonis, S. R. Harutyunyan, K.-H. Ernst, B. L. Feringa, *Nature* **2011**, *479*, 208–211.
[31] G. J. Simpson, V. García-López, P. Petermeier, L. Grill, J. M. Tour, *Nature Nanotech* **2017**, *12*, 604–606.
[32] R. Pawlak, T. Meier, *Nature Nanotech* **2017**, *12*, 712–712.
[33] A. van Venrooy, V. García-López, J. T. Li, J. M. Tour, A. V. Dubrovskiy, *J. Org. Chem.* **2020**, *85*, 13644–13654.
[34] T. Nishino, C. J. Martin, H. Takeuchi, F. Lim, K. Yasuhara, Y. Gisbert, S. Abid, N. Saffon-Merceron, C. Kammerer, G.

Rapenne, *Chemistry – A European Journal* **2020**, *26*, 12010–12018.
[35] T. Kühne, K. H. Au-Yeung, F. Eisenhut, O. Aiboudi, D. A. Ryndyk, G. Cuniberti, F. Lissel, F. Moresco, *Nanoscale* **2020**, *12*, 24471–24476.
[36] O. Krejčí, P. Hapala, M. Ondráček, P. Jelínek, *Phys. Rev. B* **2017**, *95*, 045407.
[37] T. Ikawa, S. Masuda, A. Takagi, S. Akai, *Chem. Sci.* **2016**, *7*, 5206–5211.
[38] D. Rodríguez-Lojo, D. Peña, D. Pérez, E. Guitián, *Synlett* **2015**, *26*, 1633–1637.
[39] M. Gussoni, M. Rui, G. Zerbi, *Journal of Molecular Structure* **1998**, *447*, 163–215.
[40] I. Horcas, R. Fernández, J. M. Gómez-Rodríguez, J. Colchero, J. Gómez-Herrero, A. M. Baro, *Review of Scientific Instruments* **2007**, *78*, 013705.

Entry for the Table of Contents

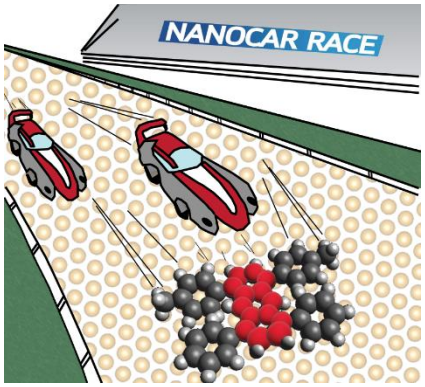

Institute and/or researcher Twitter usernames: @IMDEA_Nano, @tnicolasgarcia, @nacho_urgel, @emiliomperezlab, @davidecijalab